PHYSICAL REVIEW D **78,** 055018 (2008)

# Testing the littlest Higgs model with $T$ parity at the CERN Large Hadron Collider

Shigeki Matsumoto,[1] Takeo Moroi,[2] and Kazuhiro Tobe[3]
[1]*Department of Physics, University of Toyama, Toyama 930-8555, Japan*
[2]*Department of Physics, Tohoku University, Sendai 980-8578, Japan*
[3]*Department of Physics, Nagoya University, Nagoya 464-8602, Japan*
(Received 2 July 2008; published 25 September 2008)

In the framework of the littlest Higgs model with $T$ parity (LHT), we study the production processes of $T$-even ($T_+$) and $T$-odd ($T_-$) partners of the top quark at the Large Hadron Collider (LHC). We show that the signal events can be distinguished from the standard model backgrounds, and that information about mass and mixing parameters of the top partners can be measured with relatively good accuracies. With the measurements of these parameters, we show that a nontrivial test of the LHT can be performed. We also discuss a possibility to reconstruct the thermal relic density of the lightest $T$-odd particle $A_H$ using the LHC results and show that the scenario where $A_H$ becomes dark matter may be checked.

DOI: 10.1103/PhysRevD.78.055018 PACS numbers: 12.60.−i

## I. INTRODUCTION

The hierarchy problem in the standard model (SM) is expected to give a clue to explore physics beyond the SM. This problem is essentially related to quadratically divergent corrections to the Higgs boson mass, and it strongly suggests the existence of new physics at the TeV scale. At the new-physics scale, the problem is expected to be resolved due to the appearance of a new symmetry which controls the Higgs boson mass. With this philosophy, a lot of scenarios have been proposed so far. The most famous example is the supersymmetry (SUSY), by which quadratically divergent corrections to the Higgs boson mass are completely cancelled. Another example is the gauge-Higgs unification, by which the gauge invariance in higher dimensional space-time protects the Higgs potential from any ultraviolet (UV) divergent corrections.

In this article, we consider the third possibility, the so-called little Higgs (LH) scenario [1], in which the Higgs boson mass is controlled by a global symmetry. In this scenario, the Higgs boson is regarded as a pseudo Nambu-Goldstone boson arising from the spontaneous breaking of a symmetry. Because of the symmetry imposed, new particles such as heavy gauge bosons and top partners are necessarily introduced, and main quadratically divergent corrections to the Higgs boson mass vanish at one-loop level due to contributions of these particles. Unlike the SUSY scenario, the cancellation of the quadratic divergence is achieved only at one-loop level, thus the LH model needs a UV completion at some higher scale. However, due to the cancellation at one-loop level, the fine-tuning of the Higgs boson mass is avoided even if the cutoff scale of the LH model is around 10 TeV. As a result, the LH model solves the little hierarchy problem [2].

Unfortunately, the original LH model is severely constrained by electroweak precision measurements due to direct couplings among a new heavy gauge boson and SM particles [3]. In order to resolve the problem, the implementation of the $Z_2$ symmetry called $T$ parity to the model has been proposed [4–6]. Under the parity, almost all new particles are $T$ odd, while the SM particles are $T$ even.[1] Thanks to the symmetry, dangerous interactions stated above are prohibited [7]. Furthermore, the lightest $T$-odd particle (LTP) becomes stable, which is electrically and color neutral, and has a mass of $\mathcal{O}(100)$ GeV in many little Higgs models with $T$ parity [4]. Therefore, these models provide a good candidate for dark matter [8].[2]

In this article, we study signatures of the littlest Higgs model with $T$ parity (LHT) [5,6] at the Large Hadron Collider (LHC), which is expected to explore various new-physics models [10,11]. The LHT is the simplest model realizing the LH scenario with the $T$ parity, and it is considered to be an attractive reference model. Since the LHC is a hadron collider, new colored particles have an important role to explore physics beyond the SM. As shown in the next section, top partners are necessarily introduced in the LH models, which are responsible for the cancellation of quadratically divergent corrections to the Higgs boson mass from top-loop diagrams. Furthermore, masses of these partners are expected to be less than $\sim$1 TeV, and the partners will be copiously produced at the LHC [12]. Therefore, we consider the productions of the top partners at the LHC with a realistic simulation study, and we show that these signatures are clearly distinguishable from SM backgrounds. Furthermore, we find that it is also possible to test the LHT by investigating a nontrivial relation among the signatures. We also consider how accurately model parameters of the LHT are determined and discuss its implication to the property of the LTP dark matter such as how precisely the relic abundance of the dark matter is estimated with the LHC data.

[1]One important exception is the top partner $T_+$, which is a $T$-even new particle as shown in the next section.
[2]For UV completion of $T$-parity models, see [9].

 

This paper is organized as follows. In the next section, we briefly review the littlest Higgs model with $T$ parity paying particular attention to the gauge Higgs and top sectors of the model. We also present representative points used in our simulation study. Signatures of the LHT at the LHC are shown in Sec. III, especially focusing on the pair production of the $T$-even top partner, the single production of the $T$-even top partner, and the pair production of the $T$-odd partner. The test of the LHT is discussed in Sec. IV, where we investigate a nontrivial relation among the signatures obtained in the previous section. We also discuss the implication of the result to the LTP dark matter phenomenology. Section V is devoted to a summary.

## II. MODEL

In this section, we briefly review the littlest Higgs model with $T$ parity focusing on gauge Higgs and top sectors of the model. (For general reviews of little Higgs models and their phenomenological aspects, see [13,14].) We also present a few representative points used in our simulation study at the end of this section.

### A. Gauge-Higgs sector

The littlest Higgs model with $T$ parity is based on a nonlinear sigma model describing an SU(5)/SO(5) symmetry breaking. The nonlinear sigma field $\Sigma$ is given as

$$\Sigma = e^{2i\Pi/f}\Sigma_0, \tag{2.1}$$

where $f \sim \mathcal{O}(1)$ TeV is the vacuum expectation value of the breaking. The Nambu-Goldstone (NG) boson matrix $\Pi$ and the direction of the breaking $\Sigma_0$ are

$$\Pi = \begin{pmatrix} 0 & H/\sqrt{2} & \Phi \\ H^\dagger/\sqrt{2} & 0 & H^T/\sqrt{2} \\ \Phi^\dagger & H^*/\sqrt{2} & 0 \end{pmatrix}, \qquad \Sigma_0 = \begin{pmatrix} 0 & 0 & \mathbf{1} \\ 0 & 1 & 0 \\ \mathbf{1} & 0 & 0 \end{pmatrix}. \tag{2.2}$$

Here, we omit the would-be NG fields in the $\Pi$ matrix. An $[\mathrm{SU}(2) \times \mathrm{U}(1)]^2$ subgroup in the SU(5) global symmetry is gauged, which is broken down to the diagonal subgroup identified with the SM gauge group $\mathrm{SU}(2)_L \times \mathrm{U}(1)_Y$. Because of the presence of the gauge interactions and Yukawa interactions introduced in the next subsection, the SU(5) global symmetry is not exact, and particles in the $\Pi$ matrix become pseudo NG bosons. Fourteen ( $= 24 - 10$) NG bosons are decomposed into representations $\mathbf{1}_0 \oplus \mathbf{3}_0 \oplus \mathbf{2}_{\pm 1/2} \oplus \mathbf{3}_{\pm 1}$ under the electroweak gauge group. The first two representations are real and become longitudinal components of heavy gauge bosons when the $[\mathrm{SU}(2) \times \mathrm{U}(1)]^2$ is broken down to the SM gauge group. The other scalars $\mathbf{2}_{\pm 1/2}$ and $\mathbf{3}_{\pm 1}$ are a complex doublet identified with the SM Higgs field [$H$ in Eq. (2.2)] and a complex triplet Higgs field [$\Phi$ in Eq. (2.2)], respectively.

The kinetic term of the $\Sigma$ field is given as

$$\mathcal{L}_\Sigma = \frac{f^2}{8}\mathrm{Tr}|\partial_\mu \Sigma - i\sqrt{2}\{g(\mathbf{W}\Sigma + \Sigma\mathbf{W}^T) + g'(\mathbf{B}\Sigma + \Sigma\mathbf{B}^T)\}|^2, \tag{2.3}$$

where $\mathbf{W} = W_j^a Q_j^a$ ($\mathbf{B} = B_j Y_j$) is the $\mathrm{SU}(2)_j$ ($\mathrm{U}(1)_j$) gauge field and $g$ ($g'$) is the $\mathrm{SU}(2)_L$ ($\mathrm{U}(1)_Y$) gauge coupling constant. With the Pauli matrix $\sigma^a$, the generator $Q_j$ and the hyper-charge $Y_j$ are given as

$$Q_1^a = +\frac{1}{2}\begin{pmatrix} \sigma^a & 0 & 0 \\ 0 & 0 & 0 \\ 0 & 0 & 0 \end{pmatrix}, \qquad Y_1 = \mathrm{diag}(3, 3, -2, -2, -2)/10, \tag{2.4}$$

$$Q_2^a = -\frac{1}{2}\begin{pmatrix} 0 & 0 & 0 \\ 0 & 0 & 0 \\ 0 & 0 & \sigma^{a*} \end{pmatrix}, \qquad Y_2 = \mathrm{diag}(2, 2, 2, -3, -3)/10. \tag{2.5}$$

It turns out that the Lagrangian in Eq. (2.3) is invariant under the $T$ parity,

$$\Pi \leftrightarrow -\Omega\Pi\Omega, \qquad W_1^a \leftrightarrow W_2^a, \qquad B_1 \leftrightarrow B_2, \tag{2.6}$$

where $\Omega = \mathrm{diag}(1, 1, -1, 1, 1)$.

This model contains four kinds of gauge fields. The linear combinations $W^a = (W_1^a + W_2^a)/\sqrt{2}$ and $B = (B_1 + B_2)/\sqrt{2}$ correspond to the SM gauge bosons for the $\mathrm{SU}(2)_L$ and $\mathrm{U}(1)_Y$ symmetries. The other linear combinations $W_H^a = (W_1^a - W_2^a)/\sqrt{2}$ and $B_H = (B_1 - B_2)/\sqrt{2}$ are additional gauge bosons, which acquire masses of $\mathcal{O}(f)$ through the SU(5)/SO(5) symmetry breaking. After the electroweak symmetry breaking with $\langle H \rangle = (0, v/\sqrt{2})^T$, the neutral components of $W_H^a$ and $B_H$ are mixed with each other and form mass eigenstates $A_H$ and $Z_H$,

$$\begin{pmatrix} Z_H \\ A_H \end{pmatrix} = \begin{pmatrix} \cos\theta_H & -\sin\theta_H \\ \sin\theta_H & \cos\theta_H \end{pmatrix}\begin{pmatrix} W_H^3 \\ B_H \end{pmatrix}. \tag{2.7}$$

The mixing angle $\theta_H$ is given as

$$\tan\theta_H = -\frac{2m_{12}}{m_{11} - m_{22} + \sqrt{(m_{11} - m_{22})^2 + 4m_{12}^2}} \sim -0.15\frac{v^2}{f^2}, \tag{2.8}$$

where $m_{11} = g^2 f^2 (c_f^2 + 7)/8$, $m_{12} = g g' f^2 (1 - c_f^2)/8$, $m_{22} = g'^2 f^2 (5c_f^2 + 3)/40$, and $c_f = \cos(\sqrt{2}v/f)$. Since the mixing angle is considerably suppressed, $A_H$ is dominantly composed of $B_H$. Masses of gauge bosons are

$$m_W^2 = \frac{g^2}{4} f^2 (1 - c_f) \simeq \frac{g^2}{4} v^2, \tag{2.9}$$

$$m_Z^2 = \frac{g^2 + g'^2}{4} f^2(1 - c_f) \simeq \frac{g^2 + g'^2}{4} v^2, \tag{2.10}$$

$$m_{W_H}^2 = \frac{g^2}{4} f^2(c_f + 3) \simeq g^2 f^2, \tag{2.11}$$

$$m_{Z_H}^2 = \frac{1}{2}(m_{11} + m_{22} + \sqrt{(m_{11} - m_{22})^2 + 4m_{12}^2}) \simeq g^2 f^2, \tag{2.12}$$

$$m_{A_H}^2 = \frac{1}{2}(m_{11} + m_{22} - \sqrt{(m_{11} - m_{22})^2 + 4m_{12}^2}) \simeq 0.2 g'^2 f^2. \tag{2.13}$$

As expected from the definitions of $A_H$, $Z_H$, and $W_H$, the new heavy gauge bosons behave as $T$-odd particles, while SM gauge bosons are $T$ even.

A potential term for $H$ and $\Phi$ fields is radiatively generated as [1,8]

$$V(H, \Phi) = \lambda f^2 \mathrm{Tr}[\Phi^\dagger \Phi] - \mu^2 H^\dagger H + \frac{\lambda}{4}(H^\dagger H)^2 + \cdots \tag{2.14}$$

Main contributions to $\mu^2$ come from logarithmic divergent corrections at 1-loop level and quadratically divergent corrections at 2-loop level. As a result, $\mu^2$ is expected to be smaller than $f^2$. The triplet Higgs mass term, on the other hand, receives quadratically divergent corrections at 1-loop level, and therefore is proportional to $f^2$. The quartic coupling $\lambda$ is determined by the 1-loop effective potential from gauge and top sectors. Since both $\mu$ and $\lambda$ depend on parameters at the cutoff scale $\Lambda \simeq 4\pi f$, we treat them as free parameters in this paper. The mass of the triplet Higgs boson $\Phi$ is given by $m_\Phi^2 = \lambda f^2 = 2m_h^2 f^2/v^2$, where $m_h$ is the mass of the SM Higgs boson. The triplet Higgs boson is $T$ odd, while the SM Higgs is $T$ even.

The gauge-Higgs sector of the LHT is composed of the kinetic term of the $\Sigma$ field in Eq. (2.3) and the potential term in Eq. (2.14) in addition to appropriate kinetic terms of gauge fields $W_j^a$, $B_j$, and gluon $G$. It can be seen that the heavy photon $A_H$ is considerably lighter than other $T$-odd particles. Since the stability of $A_H$ is guaranteed by the conservation of $T$ parity, it becomes a good candidate for dark matter.

### B. Top sector

To implement $T$ parity, two SU(2) doublets $q^{(1)}$ and $q^{(2)}$ and one singlet $u_R$ are introduced for each SM fermion. Furthermore, two vectorlike singlets $\mathrm{U}^{(1)}$ and $\mathrm{U}^{(2)}$ are also introduced in the top sector in order to cancel large radiative corrections to the Higgs mass term. The quantum numbers of the particles in the top sector under the $[\mathrm{SU}(2) \times \mathrm{U}(1)]^2$ gauge symmetry are shown in Table I.

TABLE I. The quantum number for $[\mathrm{SU}(2) \times \mathrm{U}(1)]^2$ for particles in the top sector.

| | | | |
|---|---|---|---|
| $q^{(1)}$ | $(\mathbf{2}, 1/30; \mathbf{1}, 2/15)$ | $q^{(2)}$ | $(\mathbf{1}, 2/15; \mathbf{2}, 1/30)$ |
| $\mathrm{U}_L^{(1)}$ | $(\mathbf{1}, 8/15; \mathbf{1}, 2/15)$ | $\mathrm{U}_L^{(2)}$ | $(\mathbf{1}, 2/15; \mathbf{1}, 8/15)$ |
| $\mathrm{U}_R^{(1)}$ | $(\mathbf{1}, 8/15; \mathbf{1}, 2/15)$ | $\mathrm{U}_R^{(2)}$ | $(\mathbf{1}, 2/15; \mathbf{1}, 8/15)$ |
| $u_R$ | $(\mathbf{1}, 1/3; \mathbf{1}, 1/3)$ | | |

All particles are triplets under the SM $\mathrm{SU}(3)_c$ (color) symmetry.

With these particles, Yukawa interactions which are invariant under gauge symmetries and $T$ parity turn out to be

$$\mathcal{L}_t = \frac{\lambda_1 f}{2\sqrt{2}} \epsilon_{ijk}\epsilon_{xy}[(\bar{\mathcal{Q}}^{(2)}\Sigma_0)_i \tilde{\Sigma}_{jx}\tilde{\Sigma}_{ky} - \bar{\mathcal{Q}}_i^{(1)}\Sigma_{jx}\Sigma_{ky}]u_R - \lambda_2 f \sum_{n=1}^{2} \bar{\mathrm{U}}_L^{(n)}\mathrm{U}_R^{(n)} + \mathrm{H.c.}, \tag{2.15}$$

where $\mathcal{Q}^{(n)} = (q^{(n)}, \mathrm{U}_L^{(n)}, 0)^T$, $q^{(n)} = -\sigma^2(u_L^{(n)}, b_L^{(n)})^T$, and $\tilde{\Sigma} = \Sigma_0 \Omega \Sigma^\dagger \Omega \Sigma_0$. The indices $i, j, k$ run from 1 to 3, while $x, y = 4, 5$. The coupling constant $\lambda_1$ is introduced to generate the top Yukawa coupling and $\lambda_2 f$ gives the vectorlike mass of the singlet $\mathrm{U}^{(n)}$. Under $T$ parity, $q^{(n)}$ and $\mathrm{U}^{(n)}$ transform as $q^{(1)} \leftrightarrow -q^{(2)}$ and $\mathrm{U}^{(1)} \leftrightarrow -\mathrm{U}^{(2)}$, thus $T$-parity eigenstates are given as

$$q^{(\pm)} = \tfrac{1}{\sqrt{2}}(q^{(1)} \mp q^{(2)}), \qquad \mathrm{U}_{L(R)}^{(\pm)} = \tfrac{1}{\sqrt{2}}(\mathrm{U}_{L(R)}^{(1)} \mp \mathrm{U}_{L(R)}^{(2)}). \tag{2.16}$$

In terms of the eigenstates, mass terms in Eq. (2.15) are written as

$$\mathcal{L}_{\mathrm{mass}} = -\lambda_1[f\bar{\mathrm{U}}_L^{(+)} + v\bar{u}_L^{(+)}]u_R - \lambda_2 f(\bar{\mathrm{U}}_L^{(+)}\mathrm{U}_R^{(+)} + \bar{\mathrm{U}}_L^{(-)}\mathrm{U}_R^{(-)}) + \mathrm{H.c.} \tag{2.17}$$

$T$-even states $u_+$ and $\mathrm{U}_+$ form the following mass eigenstates:

$$\begin{pmatrix} t_L \\ T_{+L} \end{pmatrix} = \begin{pmatrix} \cos\beta & -\sin\beta \\ \sin\beta & \cos\beta \end{pmatrix} \begin{pmatrix} u_L^{(+)} \\ \mathrm{U}_L^{(+)} \end{pmatrix}, \qquad \begin{pmatrix} t_R \\ T_{+R} \end{pmatrix} = \begin{pmatrix} \cos\alpha & -\sin\alpha \\ \sin\alpha & \cos\alpha \end{pmatrix} \begin{pmatrix} u_R^{(+)} \\ \mathrm{U}_R^{(+)} \end{pmatrix}. \tag{2.18}$$

Mixing angles $\alpha$, $\beta$ and mass eigenvalues $m_t$, $m_{T_+}$ are given as

$$\tan\alpha = \frac{2B_tC_t}{\Delta_t - (A_t^2 + B_t^2 - C_t^2)} \simeq \lambda_1/\lambda_2,$$
$$\tan\beta = \frac{2A_tB_t}{\Delta_t - (A_t^2 - B_t^2 - C_t^2)} \simeq \frac{\lambda_1^2}{\lambda_1^2 + \lambda_2^2}\frac{v}{f}, \quad (2.19)$$
$$m_t = \frac{1}{\sqrt{2}}\sqrt{A_t^2 + B_t^2 + C_t^2 - \Delta_t} \simeq \frac{\lambda_1\lambda_2}{\sqrt{\lambda_1^2 + \lambda_2^2}}v,$$
$$m_{T_+} = \frac{1}{\sqrt{2}}\sqrt{A_t^2 + B_t^2 + C_t^2 + \Delta_t} \simeq \sqrt{\lambda_1^2 + \lambda_2^2}f,$$

where $A_t = s_f\lambda_1 f/\sqrt{2}$, $B_t = (1 + c_f)\lambda_1 f/2$, $C_t = \lambda_2 f$, and $\Delta_t = ((A_t^2 + B_t^2 + C_t^2)^2 - 4A_t^2C_t^2)^{1/2}$ with $s_f$ being $s_f = \sin(\sqrt{2}v/f)$. The $t$ quark is identified with the SM top quark, and $T_+$ is its $T$-even heavy partner. On the other hand, the $T$-odd fermions $U_{L-}$ and $U_{R-}$ form a Dirac fermion, $T_-$, whose mass is given by $m_{T_-} = \lambda_2 f$. The remaining $T$-odd quark $q_-$ acquires mass by introducing an additional SO(5) multiplet transforming nonlinearly under the SU(5) symmetry. Therefore, the mass term of the quark does not depend on $\lambda_1$ and $\lambda_2$. In this paper, we assume that the $q_-$ quark is heavy enough compared to other top partners, and that it is irrelevant for the direct production at the LHC experiment. (For the phenomenology of the $q_-$ quark, see [15].) Finally, it is worth notifying that the $T$-odd partner of the top quark ($T_-$) does not participate in the cancellation of quadratically divergent corrections to the Higgs mass term. The cancellation is achieved by only loop diagrams involving $t$ and $T_+$ quarks.

### C. Representative points

In this paper, we focus on $T_\pm$ productions at the LHC. For this purpose, we need to choose representative points to perform a numerical simulation. In order to find attractive points, we consider those consistent with electroweak precision measurements and the WMAP experiment for dark matter relics.[3]

We consider a $\chi^2$-function to choose representative points:

$$\chi^2 = \sum_i \frac{(\mathcal{O}_{\rm obs}^{(i)} - \mathcal{O}_{\rm th}^{(i)})^2}{(\Delta\mathcal{O}_{\rm obs}^{(i)})^2}, \quad (2.20)$$

where $\mathcal{O}_{\rm obs}^{(i)}$, $\mathcal{O}_{\rm th}^{(i)}$, and $\Delta\mathcal{O}_{\rm obs}^{(i)}$ are the experimental result, theoretical prediction, and the error of the observation for observable $\mathcal{O}$. We consider the following eight observables: $W$ boson mass ($m_W = 80.412 \pm 0.042$ GeV), weak mixing angle ($\sin^2\theta_{\rm eff}^{\rm lept} = 0.231\,53 \pm 0.000\,16$), leptonic width of the $Z$ boson ($\Gamma_l = 83.985 \pm 0.086$ MeV) [16], fine structure constant at the $Z$ pole ($\alpha^{-1}(m_Z) = 128.950 \pm 0.048$), top-quark mass ($m_t = 172.7 \pm 2.9$ GeV) [17], $Z$ boson mass ($m_Z = 91.1876 \pm 0.0021$ GeV), Fermi constant ($G_F = (1.166\,37 \pm 0.000\,01) \times 10^{-5}$ GeV$^{-2}$) [18], and relic abundance of dark matter ($\Omega_{\rm DM}h^2 = 0.119 \pm 0.009$) [19]. On the other hand, theoretical predictions of these observables depend on seven model parameters: $f$, $\lambda_2$, $m_h$, $\alpha^{-1}(m_Z)$, $G_F$, $m_Z$, and $m_t$. (For the detailed expressions of the theoretical predictions, see [7,8]). In order to obtain the constraint on $f$ vs the $\lambda_2$ plane, we minimize the $\chi^2$ function in Eq. (2.20) with respect to parameters $m_h$, $\alpha^{-1}(m_Z)$, $G_F$, $m_Z$, and $m_t$. In other words, we integrate out these parameters from the probability function $P \equiv e^{-\chi^2/2}$.

The result is shown in Fig. 1, where the constraints on $f$ and $\lambda_2$ at 99% confidence level ($\chi^2 = 11.34$) are depicted. The region $\lambda_2 < 1$ is not favored due to electroweak precision measurements, because a large mixing angle between $t$ and $T_+$ is predicted in this region, which leads to a significant contribution to the custodial symmetry breaking. The region $f < 570$ GeV, which corresponds to $m_{A_H} < m_W$, is not attractive because the pair annihilation of $A_H$ into the gauge-boson pair is kinematically forbidden. Here, we should comment on other parameters integrated out from the probability function. It can be easily seen that $\alpha^{-1}(m_Z)$, $G_F$, $m_Z$, and $m_t$ are almost fixed due to the precise measurements of these observables. Furthermore, once $(f, \lambda_2)$ is fixed, $m_h$ is also fixed by the WMAP observation, because the annihilation cross section of dark matter is sensitive to $m_h$. Here and hereafter, at each $(f, \lambda_2)$ point, we use values of these parameters which minimize the $\chi^2$-function. The degree of fine-tuning to set the Higgs mass on the electroweak scale is also shown

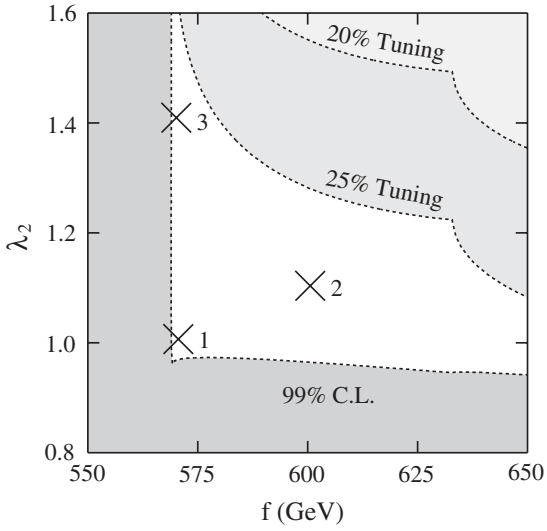


FIG. 1. Constraints to the littlest Higgs model with $T$ parity on the $f$ vs $\lambda_2$ plane at 99% confidence level. The degree of fine-tuning to the quadratic coupling of the Higgs field is also shown as light shaded regions. Cross marks 1, 2, and 3 are representative points for our simulation study.

[3]We consider the WMAP constraint only for choosing a representative point. In fact, the model does not have to satisfy the constraint, because, for instance, dark matter may be composed of other particles such as the axion.

TABLE II. Representative points used in our simulation study.

| | Point 1 | Point 2 | Point 3 |
|---|---|---|---|
| $f$ (GeV) | 570 | 600 | 570 |
| $\lambda_2$ | 1.0 | 1.1 | 1.4 |
| $\sin\beta$ | 0.20 | 0.16 | 0.11 |
| $m_h$ (GeV) | 145 | 131 | 145 |
| $m_{A_H}$ (GeV) | 80.1 | 85.4 | 80.1 |
| $m_{T_-}$ (GeV) | 570 | 660 | 798 |
| $\Gamma_{T_-}$ (GeV) | 2.3 | 2.7 | 3.6 |
| $m_{T_+}$ (GeV) | 772 | 840 | 914 |
| $\Gamma_{T_+}$ (GeV) | 11.6 | 9.6 | 5.3 |
| $\sigma(pp \to T_- \bar{T}_- + X)$ (pb) | 1.26 | 0.54 | 0.17 |
| $\sigma(pp \to T_+ \bar{T}_+ + X)$ (pb) | 0.21 | 0.13 | 0.07 |
| $\sigma(pp \to T_+ + X)$ (pb) | 0.29 | 0.15 | 0.05 |
| $\sigma(pp \to \bar{T}_+ + X)$ (pb) | 0.14 | 0.07 | 0.02 |
| $\mathrm{Br}(T_+ \to W^+ b)$ | 50.8% | 50.8% | 53.3% |
| $\mathrm{Br}(T_+ \to Zt)$ | 21.1% | 21.8% | 23.6% |
| $\mathrm{Br}(T_+ \to ht)$ | 15.8% | 17.4% | 19.1% |
| $\mathrm{Br}(T_+ \to T_- A_H)$ | 12.3% | 10.0% | 4.03% |

in the figure. As mentioned in the previous subsections, the quadratic coupling of the Higgs field $\mu^2$ is generated radiatively. One of the main contributions comes from the logarithmic divergent correction of a top-loop diagram, which yields [20]

$$\mu_t^2 = 3\frac{m_{T_+}^2}{4\pi^2}\frac{\lambda_1^2\lambda_2^2}{\lambda_1^2+\lambda_2^2}\log\left(1+\frac{\Lambda^2}{m_{T_+}^2}\right), \tag{2.21}$$

where $\Lambda \simeq 4\pi f$ is the cutoff scale of the model. We used the ratio $F = 100 \times (2m_h^2)/(\mu_t^2)\%$ to estimate the degree of fine-tuning. It can be seen that too large $f$ and $\lambda_2$ are not attractive from the view point of the fine-tuning.

Representative points used in our simulation study are shown in Fig. 1 and their details can be found in Table II. Masses of $A_H$ and $T_\pm$, cross sections for $T_\pm$ pair and single $T_+$ productions, and branching ratios of $T_+$ decay are also shown in each representative point. Note that the $T_-$ quark decays into the stable $A_H$ and the top quark with almost 100% branching ratio.

## III. SIGNALS FROM THE LHT EVENTS

Now, we consider the $T_+$ and $T_-$ production processes and their signals at the LHC. At the LHC, there are two types of $T_+$ production processes, pair production and single production processes, both of which are important. Thus, in the following, we discuss these processes separately. In addition, we also discuss the $T_-\bar{T}_-$ pair production.

### A. $T_+\bar{T}_+$ pair production

First, we discuss the $T_+\bar{T}_+$ pair production process. Once produced, $T_+$ decays as $T_+ \to bW^+$, $tZ$, $hZ$, and $A_H T_-$. Branching ratios for individual decay modes depend on the underlying parameters. However, in most of the cases, $\mathrm{Br}(T_+ \to bW^+)$ becomes larger than 0.5, and many of the $T_+$ decay into $bW^+$. Thus, in the experimental situation, the analysis using the decay mode $T_+ \to bW^+$ is statistically preferred. In such a case, the $t$ quark production events become an irreducible background. We will propose a set of kinematical cuts suitable for the elimination of the background.

For the $T_+\bar{T}_+$ production process, the most dangerous background is the $t\bar{t}$ production which has a larger cross section than the $T_+\bar{T}_+$ production.[4] Thus, we need to develop kinematical cuts to suppress the $t\bar{t}$ background. We propose to use the fact that the jets in the signal events are likely to be very energetic because they are from the decay of heavy particles (i.e., $T_+$ or $\bar{T}_+$). Consequently, the signal events are expected to have large $M_{\mathrm{eff}}$, which is defined by the sum of transverse momenta of high $p_T$ objects and missing transverse momentum $p_T^{(\mathrm{miss})}$:

$$M_{\mathrm{eff}} \equiv \sum_{\mathrm{jets}} p_T + \sum_{\mathrm{leptons}} p_T + \sum_{\mathrm{photons}} p_T + p_T^{(\mathrm{miss})}. \tag{3.1}$$

In our study, only the jets with $p_T > 30$ GeV are included into the high $p_T$ objects in order to reduce the contamination of QCD activities. We expect that the number of background events can be significantly reduced once we require that $M_{\mathrm{eff}}$ be large enough; in the following, we will see that this is indeed the case.

Once the backgrounds are reduced, the $T_+\bar{T}_+$ production events are reconstructed relatively easily. Here, we concentrate on the dominant decay mode $T_+ \to bW^+$. Then, the signal events are primarily from the process $pp \to T_+\bar{T}_+$, followed by $T_+ \to bW^+$ and $\bar{T}_+ \to \bar{b}W^-$. In particular, in order to constrain the mass of $T_+$, we use the process in which one of the $W$-boson decays hadronically while the other decays leptonically. At the parton level, the final state consists of two $b$ jets, two quark jets from $W^\pm$, one charged lepton, and one neutrino from $W^\mp$. Thus, the signal events are characterized by

(i) Several energetic jets,
(ii) One isolated lepton,
(iii) Missing $p_T$ (due to the neutrino emission).

Using the fact that, in the signal events, the missing momentum is due to the neutrino emission, we reconstruct two $T_+$ systems, which we call the $T_+^{(\mathrm{lep})}$ system and $T_+^{(\mathrm{had})}$ system; here, the $T_+^{(\mathrm{lep})}$ system ($T_+^{(\mathrm{had})}$ system) consists of high $p_T$ objects which are expected to be from $T_+$ or $\bar{T}_+$ whose decay is followed by the leptonic (hadronic) decay of the $W$ boson. To determine the $T_+^{(\mathrm{lep})}$ and $T_+^{(\mathrm{had})}$ systems, we first assume that all the missing $p_T$ is carried away by the neutrino. With this assumption, the neutrino momentum $p_\nu$ (in particular, the $z$-component of $p_\nu$) is calculated,

[4]We use the leading order calculation of the $t\bar{t}$ production cross section which is 460 pb.

requiring $(p_l + p_\nu)^2 = m_W^2$. Then, we define the $T_+^{(\mathrm{lep})}$ system as the charged lepton, reconstructed neutrino, and one of the three leading jets, while the $T_+^{(\mathrm{had})}$ system is the rest of the high $p_T$ objects. Since there is a twofold ambiguity in reconstructing the neutrino momentum, there exist six possibilities in classifying high-$p_T$ objects into $T_+^{(\mathrm{lep})}$ and $T_+^{(\mathrm{had})}$ systems. Using the fact that $T_+^{(\mathrm{lep})}$ and $T_+^{(\mathrm{had})}$ systems have the same invariant mass in the ideal case, we choose one of the six combinations with which $|M_{T_+^{(\mathrm{lep})}} - M_{T_+^{(\mathrm{had})}}|$ is minimized, where $M_{T_+^{(\mathrm{lep})}}$ and $M_{T_+^{(\mathrm{had})}}$ are invariant masses of $T_+^{(\mathrm{lep})}$ and $T_+^{(\mathrm{had})}$ systems, respectively. The distributions of the invariant masses of $T_+^{(\mathrm{lep})}$ and $T_+^{(\mathrm{had})}$ systems are expected to provide information about the $T_+$ mass.

In order to demonstrate how well our procedure works, we generate the events for the processes $pp \to T_+\bar{T}_+$ and $pp \to t\bar{t}$ (as well as those for $pp \to jT_+$ and $pp \to j\bar{T}_+$) with $\mathcal{L} = 100\ \mathrm{fb}^{-1}$. The parton-level events are generated by using the MadGraph/MadEvent packages [21], which utilizes the HELAS package [22]. Then, the Pythia package [23] is used for the hadronization processes and the detector effects are studied by using the PGS4 package [24]. In order to study the $T_+\bar{T}_+$ pair production process followed by the decay processes mentioned above, we require that the events should satisfy the following properties:

I-0: Three or more jets with $p_T > 30$ GeV, and only one isolated charged lepton.

In addition, we adopt the following kinematical cuts:

I-1: $p_{T,l} > 50$ GeV (with $p_{T,l}$ being the transverse momentum of the charged lepton),

I-2: $M_{\mathrm{eff}} > 1800$ GeV,

I-3: $|M_{T_+^{(\mathrm{lep})}} - M_{T_+^{(\mathrm{had})}}| < 100$ GeV.

Notice that the third cut is to eliminate combinatorial backgrounds. We found that, after imposing these kinematical cuts, events from the $jT_+$ and $j\bar{T}_+$ production processes are completely eliminated. Then, we calculate the distributions of $M_{T_+^{(\mathrm{had})}}$. The results are shown in Fig. 2. As one can see, the distributions have distinguishable peaks at around $M_{T_+^{(\mathrm{had})}} \sim m_{T_+}$. In addition, $t\bar{t}$ backgrounds are well below the $T_+\bar{T}_+$ signal. Thus, from the distribution of $M_{T_+^{(\mathrm{had})}}$, we will be able to study the properties of $T_+$.

One important observable from the distribution of $M_{T_+^{(\mathrm{had})}}$ is the mass of $T_+$; once we obtain the peak of the distribution, it will provide us important information about $m_{T_+}$. To see the accuracy of the determination of $m_{T_+}$, we consider the bin $\bar{M}_{\mathrm{bin}} - \frac{1}{2}\Delta M_{\mathrm{bin}} \le M_{T_+^{(\mathrm{had})}} < \bar{M}_{\mathrm{bin}} + \frac{1}{2}\Delta M_{\mathrm{bin}}$. Then, we calculate the number of events in the bin as a function of the center value $\bar{M}_{\mathrm{bin}}$ with the width $\Delta M_{\mathrm{bin}}$ being fixed. The peak of the distribution is determined by $\bar{M}_{\mathrm{bin}}$ which maximizes the number of events in the bin. We applied this procedure for $\Delta M_{\mathrm{bin}} =$ 20–60 GeV (with $\mathcal{L} = 100$ fb). Results for a set of signal and background events are shown in Table III. With repeating the Monte Carlo (MC) analysis with independent sets of signal samples, we found that the difference between the position of the peak and the input value of $m_{T_+}$ is typically 10–20 GeV or smaller. Thus, we expect a relatively accurate measurement of $m_{T_+}$.[5] In discussing the test of the

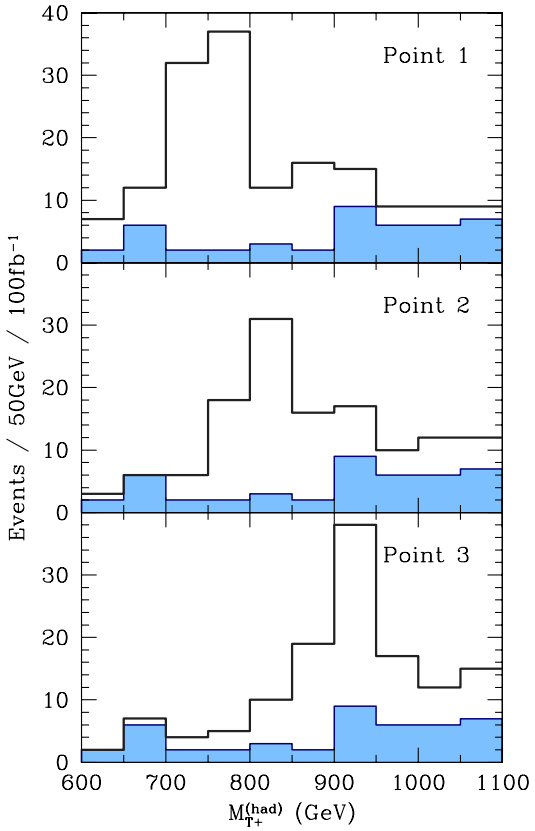


FIG. 2 (color online). Distribution of $M_{T_+^{(\mathrm{had})}}$ for Points 1–3 (from the top to the bottom) with $\mathcal{L} = 100\ \mathrm{fb}^{-1}$. The shaded histograms are the background distribution, while the solid ones are for signal + background.

TABLE III. Peak of the $M_{T_+^{(\mathrm{had})}}$ distribution for $\Delta M_{\mathrm{bin}} = 30$, 40, 50, and 60 GeV.

| | Point 1 | Point 2 | Point 3 |
|---|---|---|---|
| $\Delta M_{\mathrm{bin}} = 30$ GeV | 755 GeV | 834 GeV | 913 GeV |
| $\Delta M_{\mathrm{bin}} = 40$ GeV | 757 GeV | 839 GeV | 918 GeV |
| $\Delta M_{\mathrm{bin}} = 50$ GeV | 741 GeV | 837 GeV | 910 GeV |
| $\Delta M_{\mathrm{bin}} = 60$ GeV | 745 GeV | 847 GeV | 912 GeV |

[5]Here, the effects of the width of $T_+$ are not taken into account in our MC analysis. The width of $T_+$ is about 5–10 GeV (see Table II), which is comparable to our estimate of the uncertainty in the measurement of $m_{T_+}$. In a more detailed study, the effect of the width should be considered, which may slightly enhance the uncertainty in the determination of $m_{T_+}$.

LHT model at the LHC, we quote 10 and 20 GeV as the uncertainty of $m_{T_+}$ and discuss the implication of the measurement of $m_{T_+}$.

### B. Single production of $T_+$

As well as the pair production, the single production processes $pp \to jT_+$ and $j\bar{T}_+$ have sizable cross sections at the LHC. (Here, $j$ denotes light quark jets.) Such processes were discussed in [25] in the framework of the original littlest Higgs model without the $T$ parity, which pointed out that the discovery of $T_+$ may be possible by using this process. (See also [26].) Here, we reconsider the single production process for the test of the LHT model.

So far, we have discussed that the information about the mass of $T_+$ can be obtained by studying the $T_+\bar{T}_+$ pair production. Concerning the property of $T_+$, another important parameter is the mixing angle $\beta$, which determines the interaction between $T_+$ and weak bosons (i.e., $W^\pm$ and $Z$). Importantly, the cross sections for the processes $pp \to jT_+$ and $j\bar{T}_+$ are strongly dependent on $\beta$. In particular, since these processes are dominated by the $t$-channel $W^\pm$-boson exchange diagram (with the use of $b$- or $\bar{b}$-quark in the initial-state protons), the cross sections are approximately proportional to $\sin^2\beta$. Thus, if the cross sections of the single production processes are measured, it provides information about the mixing angle $\beta$. Although $pp \to jT_+$ and $j\bar{T}_+$ have a different cross section, their event shapes are very similar (if we neglect the charges of high $p_T$ objects). In the following, we consider how we can measure the total cross section $\sigma_{pp\to jT_+} + \sigma_{pp\to j\bar{T}_+}$.

As we have already discussed, once produced, $T_+$ dominantly decays into $b$ and $W^+$. Thus, if we consider the leptonic decay of $W^+$, there exist two energetic quarks and one charged lepton (as well as neutrino) at the parton level in the final state. Since the mass of $T_+$ is relatively large, the $b$ jet is expected to be very energetic in this case. Thus, if we limit ourselves to the cases with the leptonic decay of $W^+$, the single production events are characterized by

(i) Two (or more) jets, one of which is very energetic (due to the $b$ jet),
(ii) One isolated lepton,
(iii) Missing $p_T$ (due to the neutrino emission).

As we will see, the cross section of the background events are relatively large, so it is necessary to find a useful cut to eliminate the backgrounds as much as possible.

One of the possible cuts is to use the invariant mass of the "$bW^\pm$" system. In the signal event, the dominant source of the missing transverse momentum is the neutrino emission by the decay of $W^+$. Thus, as we have discussed in the study of the $T_+\bar{T}_+$ pair production process, we can reconstruct the momentum of the neutrino (and hence that of $W^+$). Then, we can calculate the invariant mass of the $bW^\pm$ system. In such a study, we presume that the highest $p_T$ jet is the $b$ jet because, at least at the parton level, the transverse momentum of the $b$-quark from the decay of $T_+$ is much larger than that of the extra quark. Then, since we expect that the mass of $T_+$ is well understood by the study of the $T_+\bar{T}_+$ pair production process, as discussed in the previous subsection, we only use the events with relevant value of the invariant mass to improve the signal-to-background ratio.

To estimate how well we can determine the cross section of the single production process, we generate the signal and background events for $\mathcal{L} = 100\ \mathrm{fb}^{-1}$. In [25], it was pointed out that the most serious backgrounds are from the $t\bar{t}$ production process as well as from the single production of the top quark. Thus, in our study, we take account of these backgrounds.

Once the event samples are generated, we require the following event shape:

II-0: The number of isolated lepton is 1, the number of jets (with $p_T > 30$ GeV) is 2.

In the next step, as in the case of the $T_+\bar{T}_+$ pair production, we reconstruct the momentum of the neutrino assuming that the transverse momentum of the neutrino is given by the observed missing $p_T$. In reconstructing the neutrino momentum $p_\nu$, there exists twofold ambiguity; we denote the reconstructed neutrino momenta $p_\nu^{(i)}$ $(i = 1, 2)$. For each reconstructed momentum, we calculate the invariant mass of the $bW$ system:

$$M_{bW}^{(i)} = \sqrt{(p_{j1} + p_l + p_\nu^{(i)})^2}, \tag{3.2}$$

postulating that the highest $p_T$ jet corresponds to the $b$ jet. Even though one of $M_{bW}^{(i)}$ is with the wrong $p_\nu^{(i)}$, we found that, in the signal event, the typical differences between $M_{bW}^{(1)}$ and $M_{bW}^{(2)}$ are relatively small compared to that in the background events. Thus, we reject the events unless $|M_{bW}^{(1)} - M_{bW}^{(2)}|$ is small enough.

We also comment on another useful cut to eliminate the $t\bar{t}$ background. In the $t\bar{t}$ background events, the highest $p_T$ jet is likely to be from the overlapping of several hadronic objects from different partons if the $p_T$ is required to be very large. In our analysis, the cone algorithm (with $\Delta R = 0.5$) is used to identify isolated jets. Then, if several partons from the decay of the top quark or $W$-boson are emitted in almost the same direction, hadronized objects from those partons are grouped into a single jet, which may be identified as the $b$-originated jet in the present analysis. One of the methods to reject such a background is to use the jet-mass variable, which is the invariant mass of the jet constructed from all the (observed) energy and momentum that are contained in the jet. The jet-mass of such a jet is likely to be much larger than that of the $b$ jet. As we will show, the number of background from the $t\bar{t}$ production process is significantly reduced if the jet-mass is required to be small enough.

Now, we show the results of our MC analysis. In our analysis, we use the following kinematical cuts:

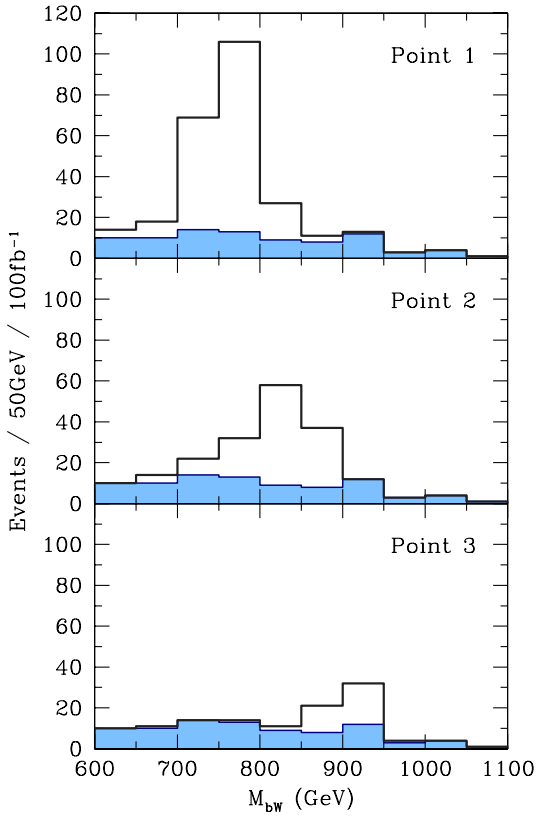


FIG. 3 (color online). Distribution of $M_{bW}$ for Points 1–3 (from the top to the bottom). The shaded histograms are the background distribution, while the solid ones are for signal + background.

II-1: $p_{T,l} > 100$ GeV, $p_T^{(\mathrm{miss})} > 100$ GeV,

II-2: $p_{T,j1} > 300$ GeV, and $M_{j1+j2} > 500$ GeV, with $M_{j1+j2}$ being the invariant mass of total jets,

II-3: $M_{j1} < 50$ GeV, with $M_{j1}$ being the jet-mass of the leading jet,

II-4: $|M_{bW}^{(1)} - M_{bW}^{(2)}| < 50$ GeV.

In Fig. 3, we plot the distribution of the "averaged" invariant mass of the $bW$ system:

$$M_{bW} \equiv \tfrac{1}{2}(M_{bW}^{(1)} + M_{bW}^{(2)}). \tag{3.3}$$

As one can see, the distribution from the signal events is peaked at around $M_{bW} \sim m_{T_+}$, while the background distribution is rather flat. In addition, at around $M_{bW} \sim m_{T_+}$, the number of signal events becomes significantly larger than that of the background, in particular, when the parameter $\sin\beta$ is relatively large. In such a case, the number of the single production events can be extracted from the distribution by using, for example, the sideband method.[6]

In Table IV, with the data for Point 2, we show the number of events in the event region, which we define $m_{T_+} - 50\ \mathrm{GeV} \le M_{bW} \le m_{T_+} + 50\ \mathrm{GeV}$, and those in the sidebands, $m_{T_+} - 150\ \mathrm{GeV} \le M_{bW} \le m_{T_+} - 50\ \mathrm{GeV}$ and $m_{T_+} + 50\ \mathrm{GeV} \le M_{bW} \le m_{T_+} + 150\ \mathrm{GeV}$, after imposing the kinematical cuts mentioned above. Assuming that the numbers of signal and background events in the signal region are determined by using the sideband events, and that the cross section for the single $T_+$ production process can be obtained from the number of events in the signal region, the single $T_+$ production cross section may be determined with the uncertainty of 10%–20%. (The uncertainty here is statistical only.)

Using the result of the $m_{T_+}$ determination with the $T_+\bar{T}_+$ pair production process, the information about the cross section can be converted to that of the mixing angle $\beta$. If the uncertainties in the theoretical calculation of the cross sections are under control, we obtain a constraint on $\beta$. Since the cross section for the single production process is proportional to $\sin^2\beta$, $\sin\beta$ is determined with the accuracy of 5%–10% if the cross section is determined with the accuracy of 10%–20%.[7] In the next section, we discuss the implication of the determination of $\beta$ at this level in testing the LHT model.

Before closing this subsection, we comment on the uncertainties which we have neglected so far. As we have mentioned, the single production process occurs by using the $b$ or $\bar{b}$ in the sea quark of the initial-state proton. Thus, for the theoretical calculation of the cross sections, it is necessary to understand the parton distribution functions for the $b$ and $\bar{b}$ quarks (as well as those of lighter quarks). Information about the parton distributions of the $b$-quark may be obtained by using the single top (and antitop) productions. As we have seen, a significant amount of single top productions occur at the LHC (which has been seen to be one of the dominant backgrounds to the single $T_+$ production process). Since the single top production also occurs by using the $b$ quark in the proton, information about the parton distribution function of $b$ will be obtained by studying the single top production process. In this paper, we do not go into the detail of such a study, but we just assume that the parton distribution function of $b$ will become available with small uncertainty once the LHC experiment will start. We also note here that it is also important to understand the efficiency to accept the single production events (as well as the background events) after the cuts, whose uncertainties have been neglected in our discussion.

[6]It should be also possible to constrain the mass of $T_+$ from the peak of the distribution of $M_{bW}$. In this paper, we will not discuss such a possibility.

[7]The cross section also depends on the mass of $T_+$. Thus, the constraint on the cross section should provide a constraint on the $\beta$ vs $m_{T_+}$ plane. In our discussion, for simplicity, we only consider the $\beta$ dependence of the cross section by using the fact that the mass of $T_+$ is expected to be determined from the $T_+\bar{T}_+$ pair production process.

TABLE IV. The number of the signal events/$t\bar{t}$ background/single top background events in the event region ($m_{T_+} - 50$ GeV $\leq M_{bW} \leq m_{T_+} + 50$ GeV) as well as in the lower and upper sidebands ($m_{T_+} - 150$ GeV $\leq M_{bW} \leq m_{T_+} - 50$ GeV and $m_{T_+} + 50$ GeV $\leq M_{bW} \leq m_{T_+} + 150$ GeV, respectively). Point 2, where $m_{T+} = 840$ GeV, is used.

| | Lower sideband | | | Event region | | | Upper sideband | | |
|---|---|---|---|---|---|---|---|---|---|
| | Signal | $t\bar{t}$ | $jt + j\bar{t}$ | Signal | $t\bar{t}$ | $jt + j\bar{t}$ | Signal | $t\bar{t}$ | $jt + j\bar{t}$ |
| II-0 | 313 | 21 706 | 13 509 | 522 | 12 585 | 8609 | 116 | 7810 | 5362 |
| II-0, 1 | 108 | 3366 | 376 | 234 | 2352 | 363 | 44 | 1747 | 237 |
| II-0, 1, 2 | 45 | 428 | 53 | 144 | 446 | 76 | 14 | 440 | 86 |
| II-0, 1, 2, 3 | 30 | 30 | 47 | 114 | 27 | 50 | 8 | 21 | 69 |
| II-0, 1, 2, 3, 4 | 21 | 12 | 18 | 84 | 11 | 12 | 2 | 3 | 16 |

### C. $T_-\bar{T}_-$ pair production

For the study of the LHT model at the LHC, it is also relevant to consider the $T$-odd top partner, $T_-$, and the lightest $T$-odd particle, $A_H$. For the study of $T$-odd particles, it is important to consider the $T_-\bar{T}_-$ pair production process, which was discussed in [27,28]. Here, we reconsider the importance of this process for the test of the LHT model.

At the LHC, $T_-$ is pair produced via $pp \to T_-\bar{T}_-$ then decays as $T_- \to tA_H$. Since $A_H$ is undetectable, the $T_-$ production events always result in missing $p_T$ events and hence the direct measurements of the masses of $T_-$ and $A_H$ are difficult.

One powerful method to study $m_{T_-}$ and $m_{A_H}$ is the so-called $M_{T2}$ analysis [29], combined with the hemisphere analysis [30]. If the $t$ and $\bar{t}$ systems are somehow reconstructed, one can constrain $m_{T_-}$ and $m_{A_H}$ from the distribution of the so-called $M_{T2}$ variable. For the event $pp \to T_-\bar{T}_-$ followed by $T_- \to tA_H$ and $\bar{T}_- \to \bar{t}A_H$, the $M_{T2}$ variable is defined as

$$M_{T2}^2(\tilde{m}_{A_H}) = \min_{\mathbf{p}_T^t + \mathbf{q}_T^{\bar{t}} + \mathbf{p}_T^{A_H} + \mathbf{q}_T^{A_H} = 0} [\max\{M_T^2(\mathbf{p}_T^t, \mathbf{p}_T^{A_H}; \tilde{m}_{A_H}), M_T^2(\mathbf{q}_T^{\bar{t}}, \mathbf{q}_T^{A_H}; \tilde{m}_{A_H})\}], \tag{3.4}$$

where the transverse mass $M_T$ is defined as

$$M_T(\mathbf{p}_T^t, \mathbf{p}_T^{A_H}; \tilde{m}_{A_H}) = \sqrt{(|\mathbf{p}_T^t|^2 + m_t^2)(|\mathbf{p}_T^{A_H}|^2 + \tilde{m}_{A_H}^2) - \mathbf{p}_T^t \mathbf{p}_T^{A_H}}, \tag{3.5}$$

with $\tilde{m}_{A_H}$ being the postulated mass of $A_H$ to calculate $M_{T2}$. In the above expression, $\mathbf{p}_T^t = (p_x^t, p_y^t, 0)$ and $\mathbf{q}_T^{\bar{t}} = (q_x^{\bar{t}}, q_y^{\bar{t}}, 0)$ are transverse momenta of $t$ and $\bar{t}$, respectively, which are obtained from the reconstructed top systems. The reconstruction of the top systems is possible with sizable efficiency by using the hemisphere method [28]. In addition, $\mathbf{p}_T^{A_H}$ and $\mathbf{q}_T^{A_H}$ are postulated transverse momenta of the final-state $A_H$ particles, which satisfy

$$\mathbf{p}_T^t + \mathbf{q}_T^{\bar{t}} + \mathbf{p}_T^{A_H} + \mathbf{q}_T^{A_H} = 0. \tag{3.6}$$

In the calculation of $M_{T2}$, $\mathbf{p}_T^{A_H}$ and $\mathbf{q}_T^{A_H}$ are varied under the above constraint to minimize the quantity in the square bracket of Eq. (3.4).

The important property of the $M_{T2}$ variable is that, if $\tilde{m}_{A_H}$ is equal to $m_{A_H}$, the upper end point of the distribution of $M_{T2}$ is given by $m_{T_-}$.[8] Thus, once many samples of $T_-\bar{T}_-$ production events become available at the LHC, it will be possible to determine the distribution of the $M_{T2}$ variable for each value of $\tilde{m}_{A_H}$. The distribution of the $M_{T2}$ variable for the $T_-\bar{T}_-$ production process was studied in [28] with the choice of $\tilde{m}_{A_H} = m_{A_H}$. In our discussion, we use the $M_{T2}$ analysis to constrain $m_{A_H}$ and $m_{T_-}$, so it is necessary to study the distribution of the $M_{T2}$ variable for various values of $\tilde{m}_{A_H}$.

To see how the distribution of the $M_{T2}$ variable depends on $\tilde{m}_{A_H}$, we generate the $T_-\bar{T}_-$ events (as well as $t\bar{t}$ backgrounds) and derive the distribution of $M_{T2}$. Here, we intend to use the events:

$$pp \to T_-\bar{T}_- \to tA_H\bar{t}A_H \to bW^+\bar{b}W^-A_HA_H \to bqq'\bar{b}q''q'''A_HA_H, \tag{3.7}$$

and we adopt the kinematical cuts used in [28]:

III-0: No isolated leptons,

III-1: $p_T^{(\mathrm{miss})} > 200$ GeV, and $p_T^{(\mathrm{miss})} > 0.2M_{\mathrm{eff}}$.

Notice that large missing $p_T$ is expected due to the emission of two $A_H$ particles. Then, in order to reconstruct two top systems, we use the hemisphere analysis with which all the high $p_T$ objects are assigned to one of two hemispheres, $H_1$ and $H_2$, so that

[8]For a general value of $\tilde{m}_{A_H}$, the upper end point of the $M_{T2}$ distribution is given by [31]

$$M_{T2}^{(\max)}(\tilde{m}_{A_H}) = \frac{m_{T_-}^2 + m_t^2 - m_{A_H}^2}{2m_{T_-}} + \sqrt{\left(\frac{m_{T_-}^2 + m_t^2 - m_{A_H}^2}{2m_{T_-}}\right)^2 + \tilde{m}_{A_H}^2 - m_t^2}.$$

This can be used to check the validity of the MC analysis.

$$\begin{cases} d(p_{H_1}, p_i) < d(p_{H_2}, p_i) & : \text{for } \forall\ i \in H_1 \\ d(p_{H_2}, p_i) < d(p_{H_1}, p_i) & : \text{for } \forall\ i \in H_2 \end{cases}, \tag{3.8}$$

where $p_{H_I}$ is the momentum of the $I$th hemisphere which is defined as

$$p_{H_I} = \sum_{i \in H_I} p_i, \tag{3.9}$$

and

$$d(p_{H_I}, p_i) = \frac{(E_{H_I} - |\mathbf{p}_{H_I}| \cos\theta_{Ii}) E_{H_I}}{(E_{H_I} + E_i)^2}, \tag{3.10}$$

with $\theta_{Ii}$ being the angle between $\mathbf{p}_{H_I}$ and $\mathbf{p}_i$. (For the details to construct the hemispheres, see [27].) In the following, the first hemisphere is defined as the one which contains the leading jet. Once two hemispheres are determined, we impose the following cuts to eliminate backgrounds:

III-2: Numbers of jets (with $p_T > 30$ GeV) in $H_1$ and $H_2$ are either equal to or smaller than 3.

III-3: $p_{T,H_I} > 200$ GeV ($I = 1, 2$), where $p_{T,H_I}$ is the transverse momentum of the hemisphere $H_I$.

III-4: $50\ \text{GeV} \le M_{H_I} \le 190\ \text{GeV} (I = 1, 2)$, where $M_{H_I}$ is the invariant mass of the $I$th hemisphere (i.e., $M_{H_I} = \sqrt{p_{H_I}^2}$).

As shown in [28], with the cuts III-0–III-3, peaks around $\sim m_t$ are obtained in the distributions of $M_{H1}$ and $M_{H2}$. Then, postulating that the momenta of $t$ and $\bar{t}$ are given by those of two hemispheres, we calculate the distribution of the $M_{T2}$ variable defined in Eq. (3.4) for several values of the postulated mass $\tilde{m}_{A_H}$. Here, we use the underlying parameters for Point 2. The results for $\tilde{m}_{A_H} = 0$, 100 GeV, and 200 GeV, for which the theoretically expected end points are 648 GeV, 664 GeV, and 708 GeV, respectively, are shown in Fig. 4. Here, the distributions shown in the figure include contributions from the $t\bar{t}$ background; however, we have checked that there is no contamination of the $t\bar{t}$ events at the end point region.

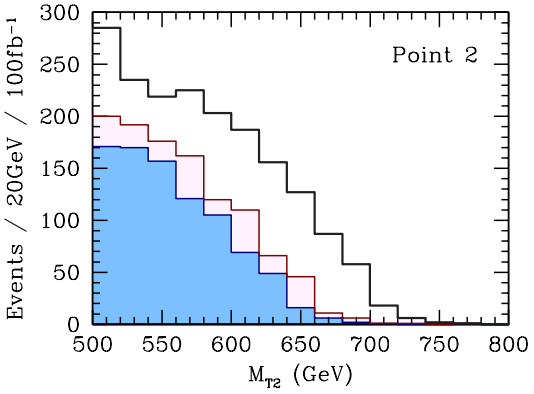


FIG. 4 (color online). Distribution of the $M_{T2}$ variable for $\tilde{m}_{A_H} = 0$ (darkly shaded: blue), 100 GeV (lightly shaded: pink), and 200 GeV (solid line).

As one can see, the position of the upper end point changes consistently with the theoretical value of the end point. Thus, by using the $M_{T2}$ variable, we expect to obtain a constraint on the $m_{A_H}$ vs $m_{T_-}$ plane, which can be transferred to a constraint on the $\lambda_2$ vs $f$ plane. In order to derive the constraint, it is necessary to understand how well the position of the upper end point can be determined. Detailed properties of the distribution of the $M_{T2}$ variable should depend on the kinematical cuts as well as on the detector performances. An extensive study of the fitting function to determine the end point is beyond the scope of this paper. Here, we simply use the quadratic function to estimate the end point. For example, for $\tilde{m}_{A_H} = 100$ GeV (for which the theoretical prediction of the end point is 664 GeV), the end point is estimated as $M_{T2}^{(\max)} = (664 \pm 9)$ GeV ($M_{T2}^{(\max)} = (676 \pm 3)$ GeV) using the data with $550\ \text{GeV} \le M_{T2} \le 650$ GeV ($580\ \text{GeV} \le M_{T2} \le 680$ GeV). Thus, in the following discussion, we adopt the error of 10–20 GeV in the determination of the end point, although a better result may be possible if a detailed study of the shape of the end point is performed.

Before closing this section, we comment on another possibility to constrain the model. As one can see from Fig. 4, we expect a significant amount of $pp \to T_-\bar{T}_-$ events. If the cross section for this process can be measured, and also if a reliable calculation of the cross section can be performed, information about the parameters of the LHT model is obtained. In particular, the cross section is determined by $m_{T_-}$, so the measurement of the cross section provides a determination of the $T_-$ mass. For such a purpose, it is crucial to understand the efficiency to accept the $pp \to T_-\bar{T}_-$ events (after kinematical cuts) as well as the background, which are unknown at this moment. Thus, it is difficult to estimate the uncertainty in the determination of $m_{T_-}$ with this method, and we do not use the information about $m_{T_-}$ in discussing the test of the LHT model.

## IV. TEST OF THE LHT MODEL

Now we discuss how and how well we can test the LHT model using the results obtained in the previous section. As we discussed in Sec. II, the LHT model is parametrized by two parameters, $f$ and $\lambda_2$. Thus, if there exists three or more observables, a nontrivial test becomes possible.

In the following, we adopt Point 2 as the underlying parameter point, and assume that $m_{T_+}$, $\sin\beta$, and the end point of the $M_{T2}$ variable can be experimentally determined as

$$m_{T_+} = [m_{T_+}]_{\text{Point 2}} \pm \delta m_{T_+}, \tag{4.1}$$

$$\sin\beta = [\sin\beta]_{\text{Point 2}} \pm \delta \sin\beta, \tag{4.2}$$

$$M_{T2}^{(\max)} = [M_{T2}^{(\max)}]_{\text{Point 2}} \pm \delta M_{T2}^{(\max)}, \tag{4.3}$$

where $[\cdots]_{\text{Point 2}}$ denotes the value in Point 2. From the discussion in the previous section, we adopt the following uncertainties of the quantities mentioned above[9]:

(i) Case 1:

$$\delta m_{T_+} = 20 \text{ GeV}, \tag{4.4}$$

$$\delta \sin\beta / \sin\beta = 10\%, \tag{4.5}$$

$$\delta M_{T2}^{(\max)} = 20 \text{ GeV}. \tag{4.6}$$

(ii) Case 2:

$$\delta m_{T_+} = 10 \text{ GeV}, \tag{4.7}$$

$$\delta \sin\beta / \sin\beta = 5\%, \tag{4.8}$$

$$\delta M_{T2}^{(\max)} = 10 \text{ GeV}. \tag{4.9}$$

In Case 2, smaller uncertainties are adopted compared to Case 1.

In Fig. 5, we show the allowed region on the $f$ vs $\lambda_2$ plane for Cases 1 and 2. As one can see, measurements of $m_{T_+}$, $\sin\beta$, and $M_{T2}^{(\max)}$ provide three different constraints on the $f$ vs $\lambda_2$ plane. It should be noticed that, because each of the constraints gives a narrow band on the $f$ vs $\lambda_2$ plane, we can quantitatively test if the observed signals are consistent with the predictions of the LHT model; if the three bands meet at a single point, as shown in Fig. 5, it gives a quantitative confirmation of the LHT model.

It is also notable that the measurements of $m_{T_+}$, $\sin\beta$, and $M_{T2}^{(\max)}$ give accurate determinations of $f$ and $\lambda_2$. For example, reading the lower and upper bounds on these parameters from the allowed region in Case 1 (Case 2), we obtain the constraints 566 GeV $< f <$ 624 GeV and $1.03 < \lambda_2 < 1.20$ (584 GeV $< f <$ 613 GeV and $1.06 < \lambda_2 < 1.15$). One of the implications is that, with the determination of $f$, we can also determine $m_{A_H}$ in the LHT model. [(See Eq. (2.13).] Since $A_H$ is a very weakly interacting particle, the direct determination of its mass is difficult as discussed in the previous section. Thus, the determination of $f$ gives important information about $m_{A_H}$.

Finally, we discuss an implication to cosmology. $A_H$ is a viable candidate of dark matter. The thermal relic density of $A_H$ strongly depends on the pair annihilation cross section of $A_H$; in the present case, $A_H$ pair-annihilates into a weak boson pair via the $s$-channel exchange of the Higgs boson. The pair annihilation cross section is obtained once $f$ and $m_h$ are known. As we have discussed, $f$ can be determined with the studies of the top partners. In addition, at the LHC, it is expected that the Higgs boson will be found and its properties will be studied in detail. For example, if $m_h = 130$–$150$ GeV, the Higgs mass will be determined with the uncertainty of $\sim$200 MeV [10,11][10]; in the following, we assume that the Higgs mass can be determined with the accuracy of 200 MeV at Point 2. Then, combining the information about the top partners and the Higgs boson from the LHC, it will become possible to reconstruct the thermal relic density of $A_H$. A comparison of the theoretically calculated relic density and observed dark matter density provides an important test of the cosmological scenario in the framework of the LHT model; if the theoretical prediction of the relic density is consistent with the dark matter density observed, it will be a strong indication of the scenario where $A_H$ is dark matter.

To see how well we can perform this test, we calculate the thermal relic density $\Omega_{A_H}$; the contours of the constant $\Omega_{A_H} h^2$ (with $h$ being the Hubble constant in units of km/

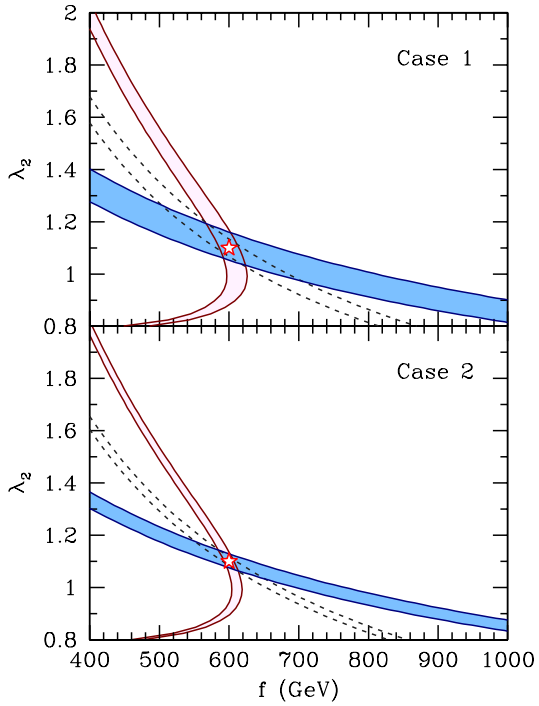


FIG. 5 (color online). Expected constraints on the $f$ vs $\lambda_2$ plane for Cases 1 and 2 (upper and lower, respectively). Point 2 is used as the underlying parameter point. Constraints from the measurements of $m_{T_+}$, $\sin\beta$, and $M_{T2}^{(\max)}$ are given by the lightly shaded (pink) region, the region between the dashed lines, and the darkly shaded (blue) region, respectively. The star in the figure is the underlying point.

[9]As we have mentioned, in Point 2, the width of $T_+$ is 9.6 GeV, which is comparable to $\delta m_{T_+}$ adopted in Case 2. Even if we use larger $\delta m_{T_+}$ for Case 2, the uncertainties in the determination of $f$ and $\lambda_2$ are almost unchanged because they can be well determined by using $\sin\beta$ and $M_{T2}^{(\max)}$.

[10]For a discussion of Higgs phenomenology in the LH models, see [32].

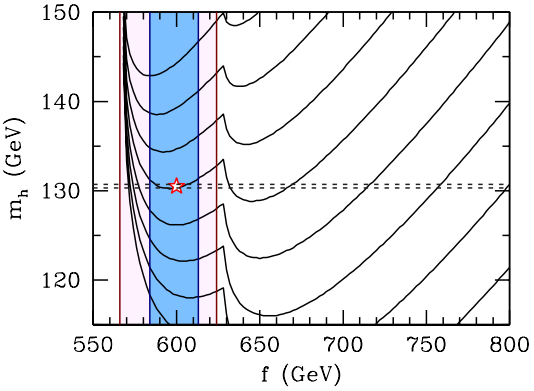


FIG. 6 (color online). Contours of the constant $\Omega_{A_H}h^2$ on the $f$ vs $m_h$ plane. Contours are for $\Omega_{A_H}h^2 = 0.06$, 0.08, 0.10, 0.12, 0.14, 0.16, 0.18, and 0.20 from above. The expected bound on $f$ is shown in the shaded region; the lightly shaded (pink) region is for Case 1 while the darkly shaded (blue) region is for Case 2. The dotted lines are the expected upper and lower bounds on the Higgs mass.

sec/Mpc) are shown in Fig. 6 on the $f$ vs $m_h$ plane. When $f \lesssim 570$ GeV, $A_H$ becomes lighter than $W^{\pm}$. In such a case, the pair annihilation cross section of $A_H$ is extremely suppressed, resulting in a very large value of $\Omega_{A_H}h^2$. On the contrary, for $f \gtrsim 570$ GeV, $\Omega_{A_H}h^2$ is found to have mild dependence on $f$ and $m_h$. In the same figure, we also show the expected constraints on $f$ and $m_h$. As one can see, determination of the $f$ parameter plays an important role in reconstructing the dark matter density. In particular, we can see that, combined with the precise measurement of the Higgs mass, $\Omega_{A_H}h^2$ can be reconstructed very accurately in Case 2 where the masses of top partners and mixing parameter $\beta$ are well determined; with the determination of $m_h$ and $f$ for Case 2 mentioned above, the density parameter is constrained to be $0.118 < \Omega_{A_H}h^2 < 0.126$. (The underlying value of $\Omega_{A_H}h^2$ is 0.120.) On the contrary, in Case 1 where the uncertainty in $f$ is relatively large, bound on the density parameter is found to be $\Omega_{A_H}h^2 > 0.118$. Thus, in such a case, $\Omega_{A_H}h^2$ cannot be bounded from above. This is mainly due to the fact that we chose the underlying value of $m_{A_H}$ close to $m_W$; with a larger value of $m_{A_H}$, a better reconstruction of $\Omega_{A_H}h^2$ is expected even with a larger uncertainty in $f$.

## V. SUMMARY

In this paper, we have studied the $T_+\bar{T}_+$ pair, single-$T_+$, and $T_-\bar{T}_-$ pair productions at the LHC in the framework of the littlest Higgs model with $T$ parity, by performing a numerical simulation on three representative points. For the $T_+\bar{T}_+$ pair production process, the main SM background comes from $t\bar{t}$ production. We have developed kinematical cuts to suppress the $t\bar{t}$ background and found that the signal events can be well extracted from the background. We have shown that an accurate determination of the mass of $T_+$ is possible. For single-$T_+$ production, we have also proposed a set of kinematical cuts to suppress the SM backgrounds which are from $t\bar{t}$ pair production and single-$t$ production and shown that the signal events can be well reconstructed. From the measurement of the single-$T_+$ production cross section as well as the measurement of $m_{T_+}$ in the $T_+\bar{T}_+$ pair production, we can obtain the information on the mixing parameter ( $\sin\beta$) between $T_+$ and the top quark. For $T_-\bar{T}_-$ pair production, studying the upper end point of the $M_{T2}$ distribution ($M_{T2}^{(\max)}$), a certain relation between $m_{A_H}$ and $m_{T_-}$ is obtained.

Since the top sector in the LHT is parametrized by two parameters, $f$ and $\lambda_2$, each measurement of these three observables provides a relation between $f$ and $\lambda_2$. We have shown that the measurements of the three observables give nontrivial determinations of the parameters $f$ and $\lambda_2$, and hence a quantitative test of the LHT model can be performed at the LHC.

In the LHT model, $A_H$ is a viable dark matter candidate. Since the thermal relic density of $A_H$ strongly depends on the pair annihilation cross section of $A_H$ into a weak boson pair via $s$-channel exchange of the Higgs boson, the masses of $A_H$ and the Higgs boson are important to calculate the thermal relic density of $A_H$. Using the facts that $A_H$ mass can be determined by the parameter $f$ and that not only the discovery of the Higgs boson but also the measurement of the Higgs mass are expected at the LHC, we have shown that the relic density of $A_H$ can be calculated very accurately by using the LHC results. This will provide an important test of the cosmological scenario where $A_H$ becomes dark matter.

Our studies here suggest not only that the LHC has a great potential to discover the heavy partner of the top quark which is responsible for the cancellation of the main quadratically divergent contribution to the Higgs mass parameter, but also that the LHC can provide important measurements of the observables that would lead us to a crucial test of the LHT model.

## ACKNOWLEDGMENTS

This work is supported in part by the Grant-in-Aid for Scientific Research from the Ministry of Education, Science, Sports, and Culture of Japan, No. 19540255 (T. M.).

[1] N. Arkani-Hamed, A. G. Cohen, and H. Georgi, Phys. Lett. B **513**, 232 (2001); N. Arkani-Hamed, A. G. Cohen, E. Katz, A. E. Nelson, T. Gregoire, and J. G. Wacker, J. High Energy Phys. 08 (2002) 021; N. Arkani-Hamed, A. G. Cohen, E. Katz, and A. E. Nelson, J. High Energy Phys. 07 (2002) 034.

[2] R. Barbieri and A. Strumia, Phys. Lett. B **433**, 63 (1998); R. Barbieri and A. Strumia, arXiv:hep-ph/0007265.

[3] C. Csaki, J. Hubisz, G. D. Kribs, P. Meade, and J. Terning, Phys. Rev. D **67**, 115002 (2003); J. L. Hewett, F. J. Petriello, and T. G. Rizzo, J. High Energy Phys. 10 (2003) 062; C. Csaki, J. Hubisz, G. D. Kribs, P. Meade, and J. Terning, Phys. Rev. D **68**, 035009 (2003); T. Gregoire, D. R. Smith, and J. G. Wacker, Phys. Rev. D **69**, 115008 (2004); M. C. Chen and S. Dawson, Phys. Rev. D **70**, 015003 (2004); Z. Han and W. Skiba, Phys. Rev. D **72**, 035005 (2005); W. Kilian and J. Reuter, Phys. Rev. D **70**, 015004 (2004).

[4] H. C. Cheng and I. Low, J. High Energy Phys. 09 (2003) 051.

[5] H. C. Cheng and I. Low, J. High Energy Phys. 08 (2004) 061.

[6] I. Low, J. High Energy Phys. 10 (2004) 067.

[7] J. Hubisz, P. Meade, A. Noble, and M. Perelstein, J. High Energy Phys. 01 (2006) 135.

[8] J. Hubisz and P. Meade, Phys. Rev. D **71**, 035016 (2005); A. Birkedal, A. Noble, M. Perelstein, and A. Spray, Phys. Rev. D **74**, 035002 (2006); M. Asano, S. Matsumoto, N. Okada, and Y. Okada, Phys. Rev. D **75**, 063506 (2007); C. S. Chen, K. Cheung, and T. C. Yuan, Phys. Lett. B **644**, 158 (2007); M. Perelstein and A. Spray, Phys. Rev. D **75**, 083519 (2007).

[9] C. T. Hill and R. J. Hill, Phys. Rev. D **75**, 115009 (2007); **76**, 115014 (2007); C. Csaki, J. Heinonen, M. Perelstein, and C. Spethmann, arXiv:0804.0622; D. Krohn and I. Yavin, J. High Energy Phys. 06 (2008) 092.

[10] ATLAS Collaboration, Report No. CERN/LHCC/99-15, 1999.

[11] CMS Collaboration, Report No. CERN/LHCC/2006-021, 2006.

[12] See, for example, G. Burdman, M. Perelstein, and A. Pierce, Phys. Rev. Lett. **90**, 241802 (2003); M. Lechowski, Cesk. Cas. Fyz. **54**, 283 (2004); H. C. Cheng, I. Low, and L. T. Wang, Phys. Rev. D **74**, 055001 (2006); C. X. Yue, L. Zhou, and S. Yang, Eur. Phys. J. C **48**, 243 (2006); K. Cheung, C. S. Kim, K. Y. Lee, and J. Song, Phys. Rev. D **74**, 115013 (2006); P. Meade and M. Reece, Phys. Rev. D **74**, 015010 (2006); M. S. Carena, J. Hubisz, M. Perelstein, and P. Verdier, Phys. Rev. D **75**, 091701 (2007); D. Choudhury and D. K. Ghosh, J. High Energy Phys. 08 (2007) 084; Q.-H. Cao and C.-R. Chen, Phys. Rev. D **76**, 075007 (2007).

[13] M. Schmaltz and D. Tucker-Smith, Annu. Rev. Nucl. Part. Sci. **55**, 229 (2005); M. Perelstein, Prog. Part. Nucl. Phys. **58**, 247 (2007).

[14] G. Burdman, M. Perelstein, and A. Pierce, Phys. Rev. Lett. **90**, 241802 (2003); **92**, 049903(E) (2004); T. Han, H. E. Logan, B. McElrath, and L. T. Wang, Phys. Rev. D **67**, 095004 (2003); M. Perelstein, M. E. Peskin, and A. Pierce, Phys. Rev. D **69**, 075002 (2004).

[15] A. Belyaev, C.-R. Chen, K. Tobe, and C.-P. Yuan, Phys. Rev. D **74**, 115020 (2006).

[16] ALEPH, DELPHI, L3, OPAL, SLD Collaborations, LEP Electroweak Working Group, SLD Electroweak Group, and SLD Heavy Flavor Group, Phys. Rep. **427**, 257 (2006).

[17] J. F. Arguin *et al.* (CDF Collaboration), arXiv:hep-ex/0507091.

[18] W. M. Yao *et al.* (Particle Data Group), J. Phys. G **33**, 1 (2006).

[19] R. R. de Austri, R. Trotta, and L. Roszkowski, J. High Energy Phys. 05 (2006) 002.

[20] A. Dobado, L. Tabares-Cheluci, and S. Penaranda, Phys. Rev. D **75**, 083527 (2007).

[21] F. Maltoni and T. Stelzer, J. High Energy Phys. 02 (2003) 027; G. C. Cho, K. Hagiwara, J. Kanzaki, T. Plehn, D. Rainwater, and T. Stelzer, Phys. Rev. D **73**, 054002 (2006); T. Stelzer and W. F. Long, Comput. Phys. Commun. **81**, 357 (1994).

[22] H. Murayama, I. Watanabe, and K. Hagiwara, Report No. KEK-91-11.

[23] H. U. Bengtsson and T. Sjostrand, Comput. Phys. Commun. **46**, 43 (1987).

[24] For an information on Pretty Good Simulation of high energy collisions (PGS4), see http://www.pysics.ucdavis.edu/~conway/research/software/pgs/pgs4-general.htm.

[25] G. Azuelos *et al.*, Eur. Phys. J. C **39S2**, 13 (2005).

[26] Q.-H. Cao, C.-S. Li, and C.-P. Yuan, arXiv:hep-ph/0612243; Q.-H. Cao, J. Wudka, and C.-P. Yuan, Phys. Lett. B **658**, 50 (2007).

[27] S. Matsumoto, M. M. Nojiri, and D. Nomura, Phys. Rev. D **75**, 055006 (2007).

[28] M. M. Nojiri and M. Takeuchi, arXiv:0802.4142.

[29] A. Barr, C. Lester, and P. Stephens, J. Phys. G **29**, 2343 (2003).

[30] See, for example, Chap. 13.4 of [11].

[31] W. S. Cho, K. Choi, Y. G. Kim, and C. B. Park, Phys. Rev. Lett. **100**, 171801 (2008); J. High Energy Phys. 02 (2008) 035.

[32] T. Han, H. E. Logan, B. McElrath, and L. T. Wang, Phys. Lett. B **563**, 191 (2003); **603**, 257(E) (2004); C.-R. Chen, K. Tobe, and C.-P. Yuan, Phys. Lett. B **640**, 263 (2006).